International Journal of Nanomedicine

Dovepress
open access to scientific and medical research

Open Access Full Text Article

ORIGINAL RESEARCH

pH-Responsive Fluorescence Enhanced Nanogel for Targeted Delivery of AUR and CDDP Against Breast Cancer

This article was published in the following Dove Press journal:
International Journal of Nanomedicine

Zhiwen Cao[1]
Wen Li[1]
Rui Liu[1]
Chenxi Li[1]
Yurong Song[1]
Guangzhi Liu[1]
Youwen Chen[1]
Cheng Lu[2]
Aiping Lu[3]
Yuanyan Liu[1]

[1]School of Chinese Materia Medica, Beijing University of Chinese Medicine, Beijing 100029, People's Republic of China; [2]Institute of Basic Research in Clinical Medicine, China Academy of Chinese Medical Sciences, Beijing 100700, People's Republic of China; [3]School of Chinese Medicine, Hong Kong Baptist University, Kowloon, Hongkong, People's Republic of China

Introduction: Auraptene (AUR), a natural bioactive prenyloxy coumarin, is a highly pleiotropic molecule that can bind to the MT1 receptor and can effectively reduce the proliferation and migration of breast cancer cells. Cisplatin (CDDP), as the first synthetic platinum-based anticancer drug, is widely used in the clinic due to its definite mechanism and therapeutic effect on diverse tumors. However, both of AUR and CDDP exhibit some disadvantages when used alone, including poor solubility, low bioavailability, lack of selectivity and systemic toxicity when they are used singly.

Methods: Therefore, the biodegradable materials hyaluronic acid (HA) and β-cyclodextrin derivative (mono-(6-amino-mono-6-deoxy)-β-CD, CD) were employed as carriers to load AUR and CDDP to form nanogel (^{CDDP}HA-CD@AUR) capable of dual-targeted delivery and synergistic therapy for breast cancer and cell imaging.

Results: With the help of the CDDP-crosslinked CD-loaded structure, the newly synthesized nanogel exhibited excellent physiological stability and fluorescence effects. The release of AUR and CDDP was affected by the pH value, which was beneficial to the selective release in the tumor microenvironment. Cell experiments in vitro demonstrated that the nanogel could be selectively internalized by MCF-7 cells and exhibited low cytotoxicity to HK-2 cells. Antitumor experiments in vivo showed that the nanogel have better antitumor effects and lower systemic toxicity.

Conclusion: Based on these, the nanogel loaded with AUR and CDDP have the potential for targeted delivery against breast cancer.

Keywords: auraptene, cisplatin, cell imaging, tumor targeting, pH-responsive

Introduction

Auraptene (AUR), also known as prenyloxy coumarin, is mainly contained in the family of Rutaceae and Apiaceae.[1] It has various pharmacological activities, such as antitumor, antibacterial, antiviral, anti-inflammatory, and antiarrhythmia, among which antitumor effect is a hotspot. AUR can reduce the viability of tumor cells, inhibit the migration and invasion of tumor cells in vitro, and alleviate the activity of matrix metalloproteinases 2 and 9.[2,3] More importantly, AUR can control the proliferation of breast cancer cells by changing the expression of genes related to the cell cycle, regulating estrogen receptors and binding to the MT1 melatonin receptor owing to the structural similarity between AUR and melatonin.[4–6] The expression of the MT1 melatonin receptor in breast cancer tissue is significantly higher than that in normal tissue.[7,8] Thus, AUR has great potential for use in the treatment of breast

Correspondence: Yuanyan Liu; Aiping Lu
Tel +86 10 84738658
Email yyliu_1980@163.com;
lap6406761l@126.com

submit your manuscript | www.dovepress.com
DovePress
http://doi.org/10.2147/IJN.S274842

cancer. Cisplatin (CDDP), a nonspecific drug for the cell cycle, has a broad spectrum of activity against different types of solid tumors. The synergistic effects of AUR and CDDP can significantly increase the expression of tumor suppressor proteins and enhance the cytotoxicity as reported in previous studies.[2,9,10] However, the poor water solubility of AUR leads to low bioavailability and little delivery to the target site, while the severe renal toxicity and low selectivity of CDDP make prioritizing chemotherapy for cancers a challenge.[3,11] Referring to the advantages of a carrier-free drug delivery system,[12] two biodegradable materials, β-cyclodextrin derivatives (mono-(6-amino-mono-6-deoxy)-β-CD, CD) and hyaluronic acid (HA), were selected as carriers in this experiment to load AUR and CDDP against breast cancer, overcoming the problems of solubility, selectivity, and system toxicity.

CD, a biodegradable amphiphilic host molecule, has been extensively used to improve the solubility, stability and bioavailability of drugs through the formation of inclusion complexes.[11,13] The hydrophobic inner cavity can form a stable host-guest inclusion complex with hydrophobic molecules of AUR.[11,14] In addition, CD can affect the photochemical and photophysical properties of guest molecules due to the limitation of the shape and size of the inner cavity.[15,16] Coumarin compounds have better optical characteristics and quantum yields, and have been widely developed as fluorescent probes.[17–19] The electron-donating group at the 7-position of AUR contributes to increased photostability. Therefore, CD was not only used to load AUR to increase its solubility, stability, and bioavailability, but also to enhance its fluorescence intensity for cell imaging.[20,21]

HA, a biodegradable polysaccharide, has biocompatibility, biodegradability, and nonimmunogenicity properties.[12] As a water-soluble natural polysaccharide, it has been widely explored and applied in the construction of nanoscale drug delivery systems.[13] Moreover HA can be recognized by six types of receptors: CD44, RHAMM, lymphatic vessel endothelial HA receptor-1, hyaluronan receptor for endocytosis, layilin, and Toll-like receptor 4, which make it used as a cancer-cell-specific ligand to achieve the purpose of targeted delivery.[12,22,23] Among them, CD44 and RHAMM have been confirmed to be overexpressed on the surface of various cancer cells, and they can recognize HA to enter cells by endocytosis. In particular, HA is an anionic natural linear material containing a large number of carboxyl and hydroxyl groups, which can be linked to specific moieties.[24] Taking these advantages, CD was modified on HA by amide bond, and amide bond can be broken under the action of proteases and acidic conditions in the lysosome.[25] CDDP has been modified on HA through chelation.[26] By anchoring the drug to the polymer matrix through the pH-response linkage, the nanocarrier can be stabilized under normal physiological conditions while dispersed in the acidic microenvironment of the tumor and then release the drug. Such a pH-responsive cross-linked structure can effectively deliver the cargos to the specific site and improve the antitumor effect.[13]

Based on the above considerations, we successfully synthesized a pH-responsive fluorescence enhanced nanogel (^{CDDP}HA-CD@AUR) for dual-targeted on breast cancers and cell imaging. The active targeting of HA receptors combined with AUR-specific ligands forms a dual-targeted nanogel to improve the internalization of ^{CDDP}HA-CD@AUR by breast tumor cells, while the fluorescence properties of AUR can track the selectivity and distribution of ^{CDDP}HA-CD@AUR in cells. CDDP, as a crosslinker and therapeutic drug, was connected to the carboxyl group of HA through chelation to stabilize the nanogel, while the cross-linked structure enabled the drug to have a pH-responsive release capability. Meanwhile, the effect and uptake behavior of ^{CDDP}HA-CD@AUR were investigated in MCF-7 and HK-2 cells in vitro, and its antitumor effect and systemic toxicity following intravenous administration were determined in tumor-bearing mice in vivo.

Materials and Methods

Reagents and Materials

Sodium hyaluronate (HA, MW=90 kDa) was purchased from Bloomage Freda Biopharm. N-hydroxysuccinimide (NHS) and 1-Ethyl-3(3-dimethylaminopropyl) carbodiimide (EDC) were obtained from Macklin. Auraptene (AUR), mono-(6-amino-mono-6-deoxy)-β-CD (CD) and cisplatin (CDDP) were purchased from Shanghai Yuanye Bio-Technology Co., Ltd. Dimethyl sulfoxide (DMSO) and 4′-6-diamidino-2-phenylindole dihydrochloride (DAPI) were purchased from Sigma-Aldrich. Cell Counting Kit-8 (CCK-8) was obtained from Dojindo Laboratories. Fetal bovine serum (FBS) was obtained from Gibco Laboratories, and DMEM/HIGH Glucose medium, DMEM-H/F-12 medium and 1% antibiotics (penicillin 100 U/mL, and streptomycin 100 mg/mL) were purchased from HyClone Laboratories. Human breast cancer MCF-7 cells were obtained from BeNa Culture Collection

(BNCC). HK-2 cells were purchased from American Type Culture Collection (ATCC).

Preparation of ^{CDDP}HA-CD@AUR Nanogel

The synthesis of the ^{CDDP}HA-CD@AUR nanogel was obtained by a three-step reaction. First, the carrier of HA-CD was prepared. The connection of HA and CD occurs through the reaction of the carboxyl group of HA and the amino group of CD to form an amide bond. Then, HA-CD was used to load AUR to obtain HA-CD@AUR. This process was realized by loading the hydrophobic guest molecule AUR into the hydrophobic inner cavity of CD. Finally, the ^{CDDP}HA-CD@AUR nanogel was obtained by the chelate interaction of CDDP and HA. Specifically, sodium hyaluronate powder (50 mg) was dissolved in deionized water (15 mL) and stirred well to disperse. Then EDC (83.8 mg, 0.438 mmol) and NHS (50.3 mg, 0.438 mmol) were added to the above solution. After stirring for 30 minutes at room temperature, 5 mL of CD (281.4 mg 0.25 mmol) aqueous solution was slowly added to the reaction solution, and the reaction was stirred at room temperature for 24 h. Finally, the reaction solution was dialyzed for 3 days in deionized water to remove excess CD and catalysts (molecular weight cut-off (MWCO) = 3500 Da). To obtain HA-CD@AUR, AUR (37.3 mg, 0.125 mmol) was dissolved in ethanol (5 mL) and slowly dropped into the dialysate of HA-CD under darkness and stirred at 50 °C for 4 h. Similarly, the solution was dialyzed in deionized water for 5 days (MWCO=3500 Da). Finally, the dialysate was lyophilized to obtain a white powder HA-CD@AUR. From HA-CD @AUR to ^{CDDP}HA-CD@AUR, to increase the load of CDDP, the amount of HA needs to be increased. Another 250 mg of HA was dissolved in 30 mL of deionized water. Then HA-CD@AUR was dissolved in deionized water (10 mL) and added slowly, with vigorous stirring to achieve uniform dispersion. The CDDP was dissolved in deionized water (10 mL) according to the molar concentration ratio (10:1) of [COOH]/[CDDP] and then slowly dropped into the solution mentioned above with vigorous stirring. After 48 h, the solution was dialyzed and lyophilized to obtain the ^{CDDP}HA-CD@AUR nanogel. This part of the experiment should be completed under darkness.

Hemolytic Tests

One milliliter of rabbit blood was obtained using a blood collection tube containing ethylenediamine tetracetic acid, and 5 mL of physiological saline (0.9% sodium chloride) was added to the blood for dilution. The blood sample was centrifuged at 2500 r/min for 5 minutes at 4 °C to separate blood red blood cells (RBCs) from the plasma. The RBCs were washed three times and then diluted to a concentration of 2% (V/V) with physiological saline. RBCs (2%) were added to the ^{CDDP}HA-CD@AUR solution at a predetermined concentration. Then, 2% RBCs were added to physiological saline and deionized water as positive and negative controls, respectively. All the solutions were mixed and placed in an incubator at 37 °C for 2 h and then centrifuged at 2500r/min for 5min in a centrifuge to collect the supernatant. One hundred microliters of the supernatant was transferred to a 96-well plate, and the absorbance was measured at 540 nm using a microplate reader. The hemolysis rate was calculated according to the following formula: hemolysis rate (%) = $(A_{sample} - A_{negative\ group})/(A_{positive\ control} - A_{negative\ group}) \times 100\%$. A_{sample}, $A_{negative\ group}$, and $A_{positive\ control}$ represent the absorbance values of different concentration samples and the negative and positive controls, respectively.

Characterization of ^{CDDP}HA-CD@AUR

The conjugation of CDDP and CD was measured by Fourier transform infrared spectroscopy (FT-IR, Thermo Nicolet is10). The morphology and stability of the nanogel were observed with a transmission electron microscope (TEM, HT7700). To observe the morphological changes of the nanogel in PBS solutions of different pH values, the nanogel was placed in PBS solutions of different pH values (pH 5.5, 6.8 and 7.4), sonicated for 5 minutes to promote dispersion, and then the morphological changes of the nanogel at 6 and 24 h were observed by TEM. To observe the results of the synthesis, the zeta potential changes of HA-CD@AUR and ^{CDDP}HA-CD@AUR were observed by Zetasizer. The average particle size was also measured by DLS. The fluorescence intensities of AUR, CD@AUR, and ^{CDDP}HA-CD @AUR were determined with a fluorescence spectrophotometer (PerkinElmer LS45). All compounds were dissolved in DMSO and diluted with PBS (V_{DMSO}/V_{PBS}=2/8).

In vitro Drug Release

To evaluate the release effect of AUR and CDDP from the nanogel, 3 mg of ^{CDDP}HA-CD@AUR was dissolved in

2 mL PBS at different pH values (pH 5.5, 6.8 and 7.4), placed in a cellulose dialysis membrane tube (MWCO=3.5 kDa), and dialyzed in 30 mL PBS with related pH values. The conditions were controlled at 37 °C, 50r/min. Then, 300μL solutions were taken at 0, 0.5, 1, 2, 3, 4, 6, 24, 48h and replaced with the same volume of PBS. The amount of AUR was determined by microplate reader at 330 nm. CDDP was released from nanogels using o-phenylenediamine colorimetry according to a previously published protocol.[27,28] In brief, the sample solution was diluted to 500 μL, 2 mg/mL of o-phenylenediamine solution was added, and the mixture was heated in a water bath for 10 minutes. After cooling, it was measured at 703 nm with a microplate reader.

Cell Culture

Human breast cancer MCF-7 cells and human kidney 2 (HK-2) cells were cultured in CM1-1 medium (90% DMEM/HIGH glucose medium containing 10% (V/V) fetal bovine serum) and CM9-1 medium (90% DMEM-H/F-12 containing 10% (V/V) fetal bovine serum), respectively, in an atmosphere of 5% (V/V) CO2 at 37 °C. The medium was replaced every two days, and the cells were washed three times with PBS and then digested by trypsinization.

Cellular Uptake

The cellular uptake was observed by confocal laser scanning microscopy (CLSM). CLSM was used to verify the feasibility of cell imaging and to compare the uptake of tumor cells and normal cells. Briefly, 500 μL of MCF-7 cells and HK-2 cells (1×10^4) was added to glass bottom dishes from the middle, and incubated in the incubator for 2h to adhere to the wall, and then the medium was filled to 2 mL and incubated for 24h. Then, MCF-7 cells were treated with AUR, CD@AUR and ^{CDDP}HA-CD@AUR, and HK-2 cells were treated with ^{CDDP}HA-CD@AUR. After 4 hours, the culture medium was removed, and the cells were washed two times with PBS. After that, all cells were stained with 4′, 6-diamidino-2-phenylindole (DAPI, 2 mL) in the incubator for 15 minutes. Subsequently, the cells were washed three times with PBS and imaged by CLSM to observe the difference in fluorescence intensity of AUR, CD@AUR and ^{CDDP}HA-CD@AUR in MCF-7 cells, and the difference in ^{CDDP}HA-CD@AUR uptake by MCF-7 cells and HK-2 cells (488 nm was applied to excite AUR).

In vitro Cytotoxicity 66

HK-2 cells were often used to study the nephrotoxicity of CDDP. Therefore, the in vitro cytotoxicity of ^{CDDP}HA-CD@AUR was assessed by HK-2 (normal cells), MDA-MB-231 (tumor cells) and MCF-7 cells (tumor cells). The toxicity of ^{CDDP}HA-CD@AUR, free CDDP and the mixture of CDDP and AUR (wt/wt = 1:2) to HK-2 cells MDA-MB-231 cells, and MCF-7 cells was assessed by the CCK-8 method. Briefly, MCF-7, MDA-MB-231 and HK-2 cells were cultured in a 96-well plate at a density of 1×10^4 cells/well for 24 h, and then the cells were treated with different concentrations of ^{CDDP}HA-CD@AUR, CDDP, and the mixture. After 24 h, 10 μL of CCK-8 solution was added to each well, incubated in the incubator for 2 h, and the absorbance was measured at 450 nm with a microplate reader. All samples were repeated three times. Similarly, MCF-7, MDA-MB-231 and HK-2 cells were incubated with the nanogel (equivalent CDDP concentration of 20 μg/mL) to further detect cytotoxicity in more time intervals, and CCK-8 experiments were performed after 24, 48 and 72 hours.

In vivo Antitumor Efficacy

Female BALB/C nude mice (20 ± 1 g) were purchased from Beijing Vital River Laboratory Animal Technology Co., Ltd (SCXK (jing) 2016–0011). The protocol of this study was authorized by the Research Ethics Committee of Institute of Basic Theory of Chinese Medicine, China Academy of Chinese Medical Sciences (the rodent license NO. SYXK 11–00-0039) and experiments were carried out in accordance with the Guide for the Care and Use of Laboratory Animals. The breast cancer model was established by subcutaneous injection of MDA-MB-231 cells (2×10^6, dispersed in 0.1 mL of PBS solution). When the average tumor volume was $50mm^3$, the mice were randomly divided into three groups (n=5). Each group was injected with saline, free CDDP plus AUR and ^{CDDP}HA-CD@AUR through the tail vein on days 0, 3, 6, 9, 12, and 14. On days 0, 3, 6, 9, 12, 14, and 16, the mice were weighed, and the tumor volume was measured with a Vernier caliper. Tumor volume (V, mm^3) was calculated by the formula $V=A\times B^2/2$ (A (mm) and B (mm) represent the largest and smallest diameters of the tumor, respectively).

Histological Examination

After the last weighing and measurement of tumor volume, the tumor tissue and major organs (heart, liver, spleen, lungs, and kidneys) of the mice were dissected for histopathological examination. The samples were fixed in 4% PBS-buffered

paraformaldehyde for 48 hours. Sequentially, low- to high-concentration alcohol is used as a dehydrating agent to remove moisture from the tissue. Then the tissue was embedded in paraffin, sliced, and baked. After dewaxing and dehydration by dimethylbenzene and absolute ethanol, the slices were stained with hematoxylin for 5 minutes, washed twice with 0.2% hydrochloric acid and alcohol solution, stained with eosin for 3 minutes, and washed twice with 95% ethanol. Finally, the slices were washed with absolute ethanol, made transparent with dimethylbenzene, fixed with neutral gum and detected by a microscope.

Statistical Analysis

Statistical analyses were conducted using SPSS 16.0 and Origin 8.5 software. All results were represented as the mean ± standard deviation (SD). The Student's *t*-test was employed for statistical analysis of group differences. $P < 0.05$ was considered statistically significant (*$p < 0.05$, **$p < 0.01$ and ***$p < 0.001$).

Results and Discussion

Synthesis of ^{CDDP}HA-CD@AUR

As shown in Scheme 1, HA contains abundant carboxyl groups, which can be well amidated with the amino groups of CD under the catalysis of EDC and NHS. The hydrophobic inner cavity of CD can form inclusion complexes with AUR, ensuring that AUR was loaded into the nanogel without chemical modification. CDDP as a crosslinker was connected to the carboxyl group of HA to form a nanogel through chelate interactions.

To evaluate the success of the nanogel synthesis, the conjugate structure of the nanogel was observed by FTIR. As shown in Figure 1, upon observing the infrared spectra of the mixtures (AUR, CDDP, CD, and HA) and the nanogel, it can be seen that there were obvious changes, and some peaks have an enhanced phenomenon. The absorption peaks at 1645cm^{-1} and 1560cm^{-1} were significantly enhanced. 1645cm^{-1} is related to stretching vibration of amide I (NC = O), imine bond and metal ion coordination bond, and 1560cm^{-1} belongs to the bending vibration of amide II (CN-H), which illustrates the formation of new amide bond and ion coordination bond.

The zeta potentials of the intermediate product HA-CD @AUR and the final product ^{CDDP}HA-CD@AUR are −23.7 and −10.7 mV, respectively. The change in zeta potential may be related to the occupation of carboxyl groups by CDDP. The negative surface potential of the nanogel indicates good dispersion stability. In addition, the

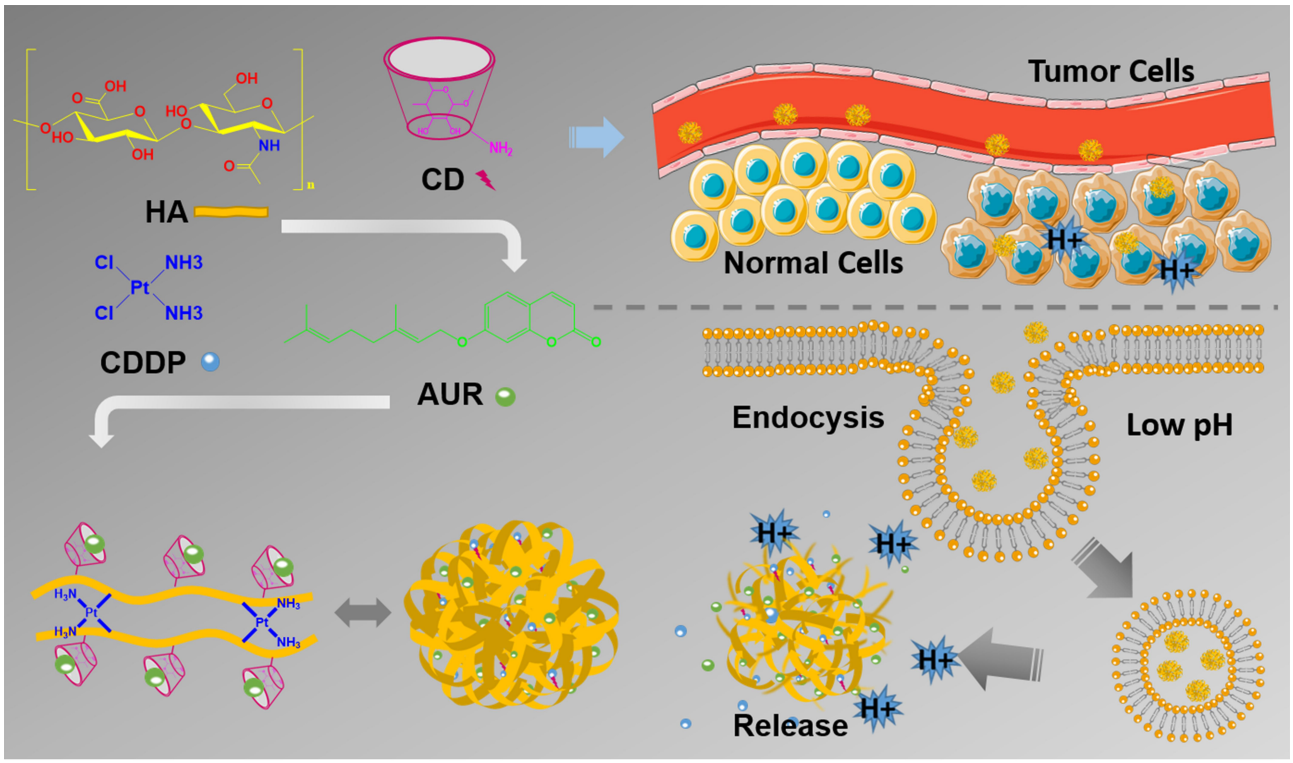

Scheme 1 Schematic diagram for nanogel synthesis, tumor targeting, cell internalization, and pH-responsive drug release.

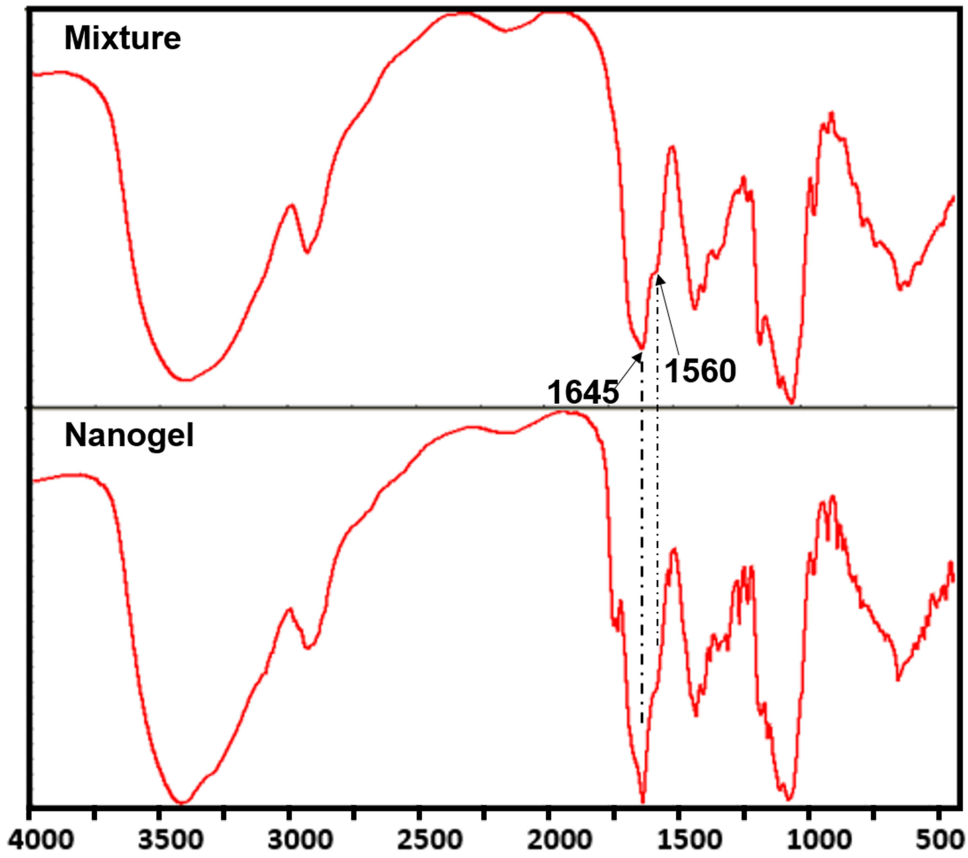

Figure 1 FT-IR spectra of the mixture (HA, CD, AUR and CDDP) and the nanogel.

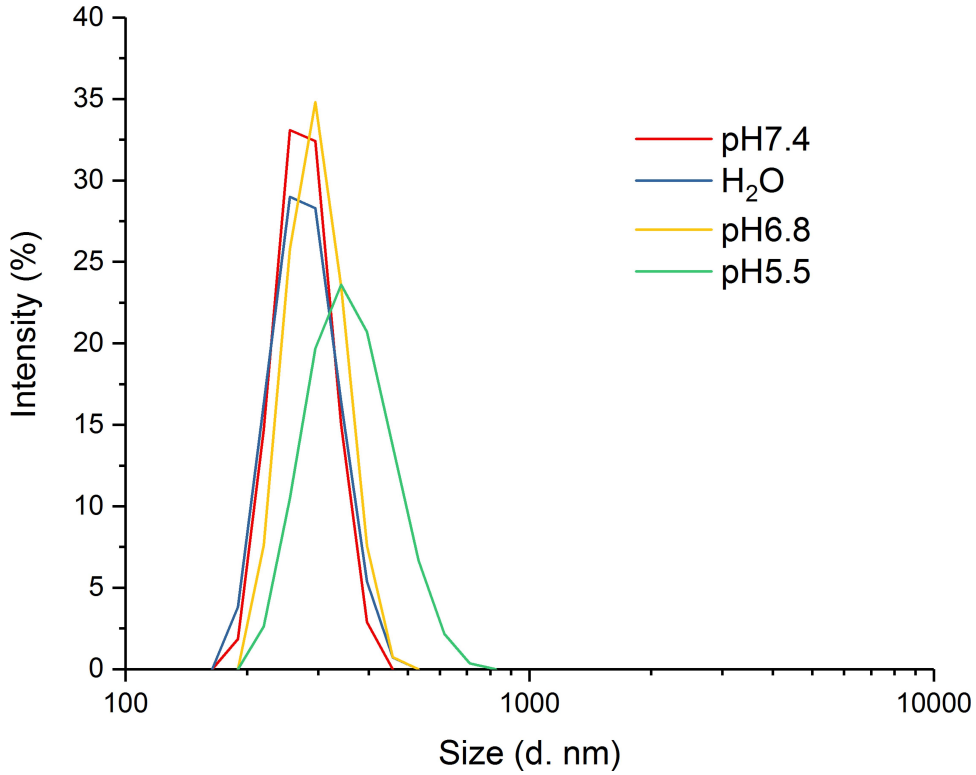

Figure 2 The particle size distribution of the nanogel in H_2O and PBS solutions (pH 7.4, 6.8 and 5.5).

slightly negative surface charge of the nanogel is beneficial for in vivo applications due to the potential of protein resistance in the blood circulation and reduces the undesirable clearance of the reticuloendothelial system.[29–31]

Size and Morphological Characteristics of the Nanogel

To detect the size of the nanogel in different solvents, the nanogel was dispersed in water and PBS solutions with different pH values, and samples were sent for detection after 2 h. In this study, to simulate different acidic environments in the body, pH 5.5, 6.8, and 7.4 PBS solutions were selected to simulate the acidic environment of lysosomes in tumor cells, the acidity of tumor tissue, and the normal physiological environment.[32] As shown in Figure 2, the particle size distribution of the nanogel in water and PBS solution at pH 7.4 was 255 nm, while the particle sizes of the nanogel in PBS solutions at pH 6.8 and pH 5.5 were 295 nm and 342 nm, respectively. The increase in the volume of nanogel under acidic conditions may be related to the weakening of chelation after protonation of carboxyl groups. The result of sample swelling under acidic conditions is conducive to the release of the drug. It also shows that the nanogel has a certain stability under normal physiological conditions.

To further observe the morphological and size changes of the nanogel under different acidic conditions, we also incubated the nanogel with PBS solutions of different pH values. As shown in Figure 3, the nanogel was dispersed in PBS solutions of different pH values, and the samples were taken at 6 h and 24 h and observed under TEM. It can be seen from the figure that the edges of the nanogel began to become blurred in the acidic environment of pH 6.8 and 5.5 at 6 h. However, when the nanogel was incubated in PBS solution for 24 h, the difference was more obvious. In the pH 6.8 and pH 5.5 groups, especially the pH 5.5 group, the nanogel was completely decomposed, and only the chaotic structure can be seen. The phenomenon indicates that the nanogel has good physiological stability and can rapidly swell and decompose in tumor tissues.

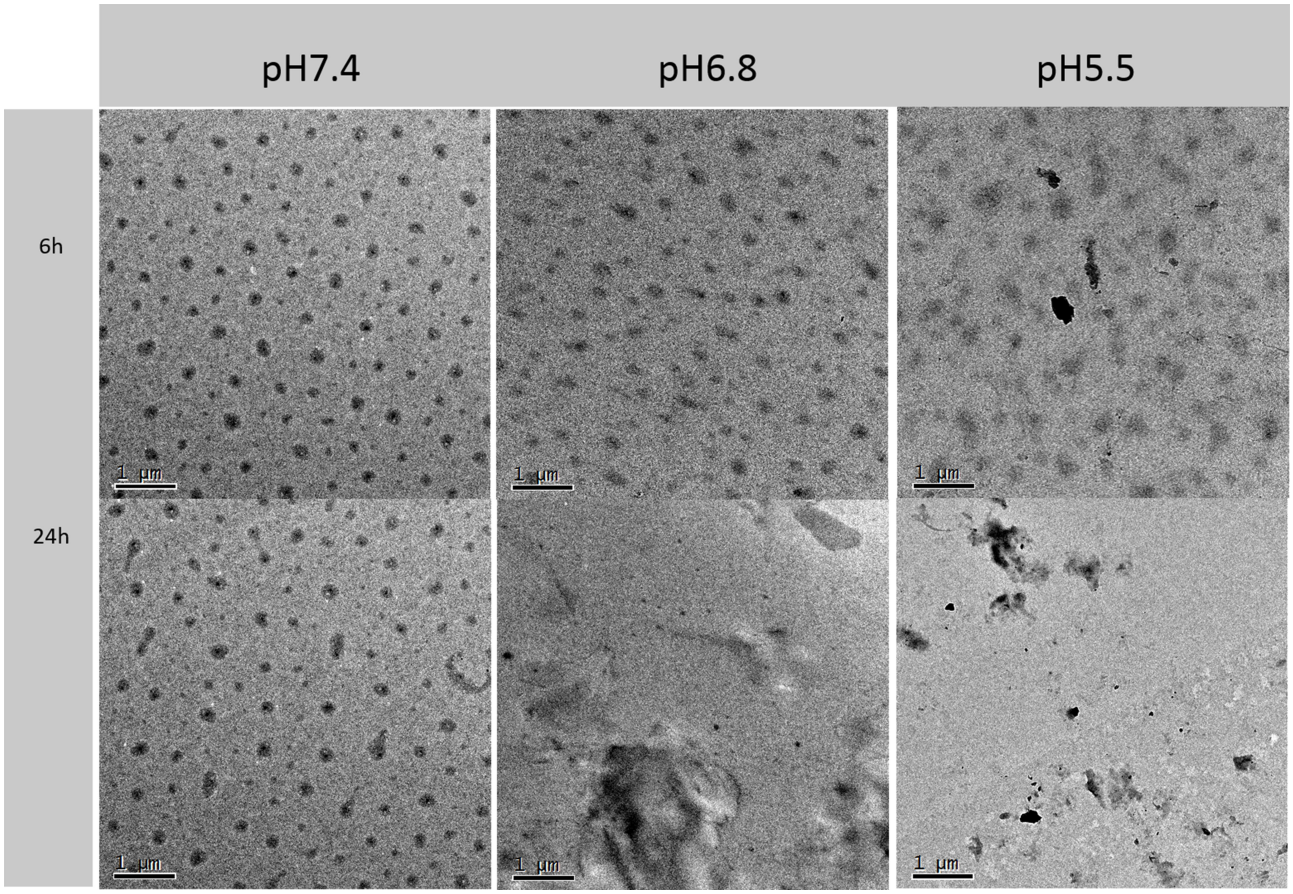

Figure 3 TEM images of the nanogel in PBS buffer at different pH values. Scale bar: 1 μm.

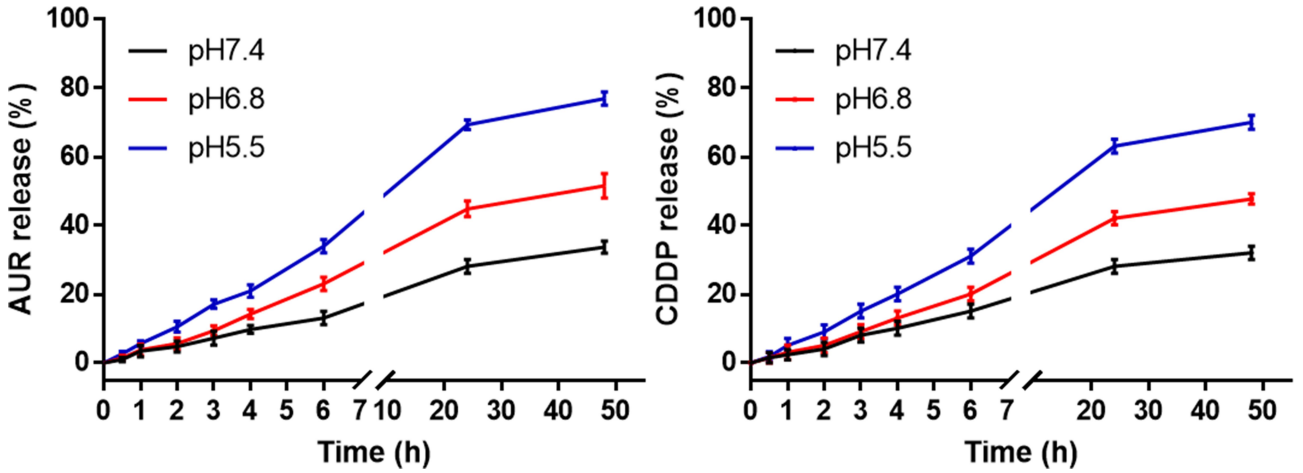

Figure 4 In vitro release of drugs in PBS buffers of different pH values.

Drugs Loading and in vitro Drug Release

The free CDDP and AUR were collected during the preparation of the nanogel and quantified by UV-vis spectroscopy. The drug loading efficiency (DLE) of the CDDP and AUR reached 55.1% and 64.9%, respectively. The release of AUR and CDDP from the nanogel by dialysis method was performed in PBS solutions at pH 5.5, 6.8 and 7.4. As depicted in Figure 4, the release of AUR gradually increases with time and releases quickly at first and then gradually slows down. The release trend of AUR was similar under the three acidic conditions, but it is worth noting that the release of AUR was affected by the pH value. At 48 h, the release of AUR at pH 5.5 reached 78%, while at pH 6.8 and pH 7.4, only 52% and 34%, respectively, were released from the nanogel. These results indicate that the release of AUR is affected by the pH value. The release trend of CDDP from the nanogel was similar to that of AUR, but its release rate was obviously slower. After 48 h of incubation, only 32% of CDDP was released under normal physiological conditions, while the release

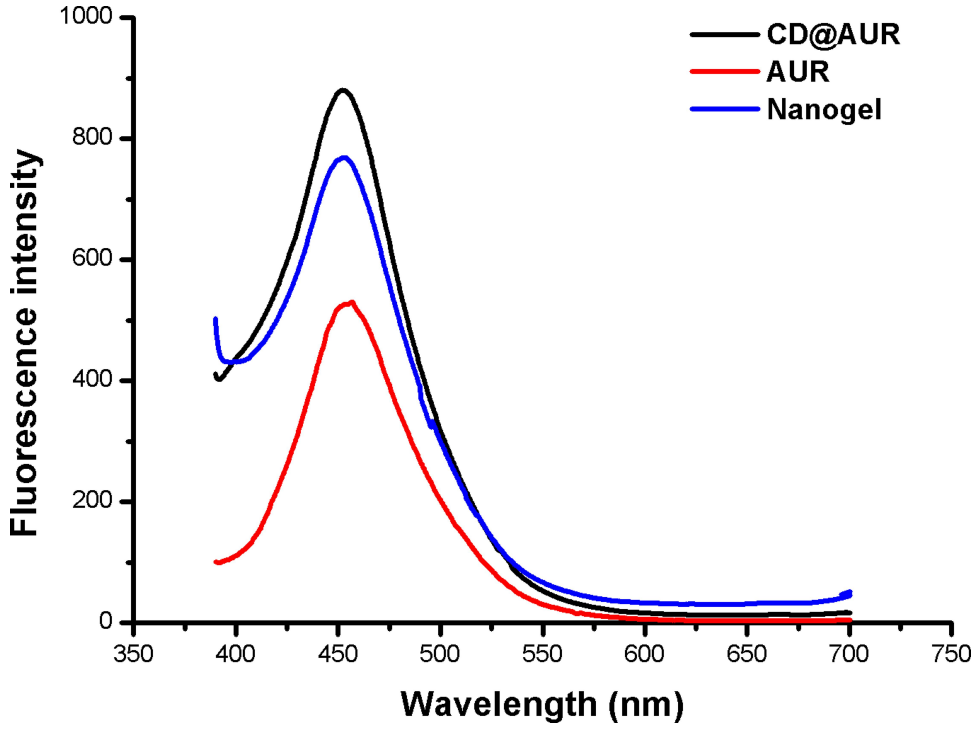

Figure 5 Fluorescence spectra of AUR, CD@AUR and the nanogel.

of CDDP reached 48% and 71% at pH 6.8 and pH 5.5, respectively.

Since the weakening of chelation under acidic conditions, the release of CDDP from the nanogel was affected by pH value.[26] The release of AUR may be attributed to the varied cross-linking degree of the nanogel.[33] With the weakening of chelation under acidic conditions, it will result in the dispersion of the nanogel, and the reduced steric hindrance will help the release of AUR. Besides, protonation of AUR's ether bonds and amide bond cleavage under acidic conditions may also be a cause of AUR release from the nanogel.[34–36] Taken together, the release of AUR and CDDP were obviously affected by the acidic environment, and the behavior of differential release in physiological conditions and tumor environment helped to improve the selectivity of drugs.

Optical Properties and Cell Internalization

Considering the high molar absorption coefficient and quantum yield of coumarins.[37] The optical characteristics of AUR, CD@AUR and ^{CDDP}HA-CD@AUR were detected by fluorescence spectroscopy. As depicted in Figure 5, the emission peaks of all three appear at 453 nm at the excitation wavelength of 370 nm and the fluorescence intensity of CD@AUR and nanogel were enhanced significantly.

The increase in fluorescence intensity promoted us to further explore their effects on cells. As shown in Figure 6, after incubation with AUR, CD@AUR, and ^{CDDP}HA-CD@AUR at 37 °C for 4 h (the final AUR concentration was 25 μg/mL), MCF-7 cells exhibited green fluorescence under CLSM. Compared with CD@AUR and ^{CDDP}HA-CD

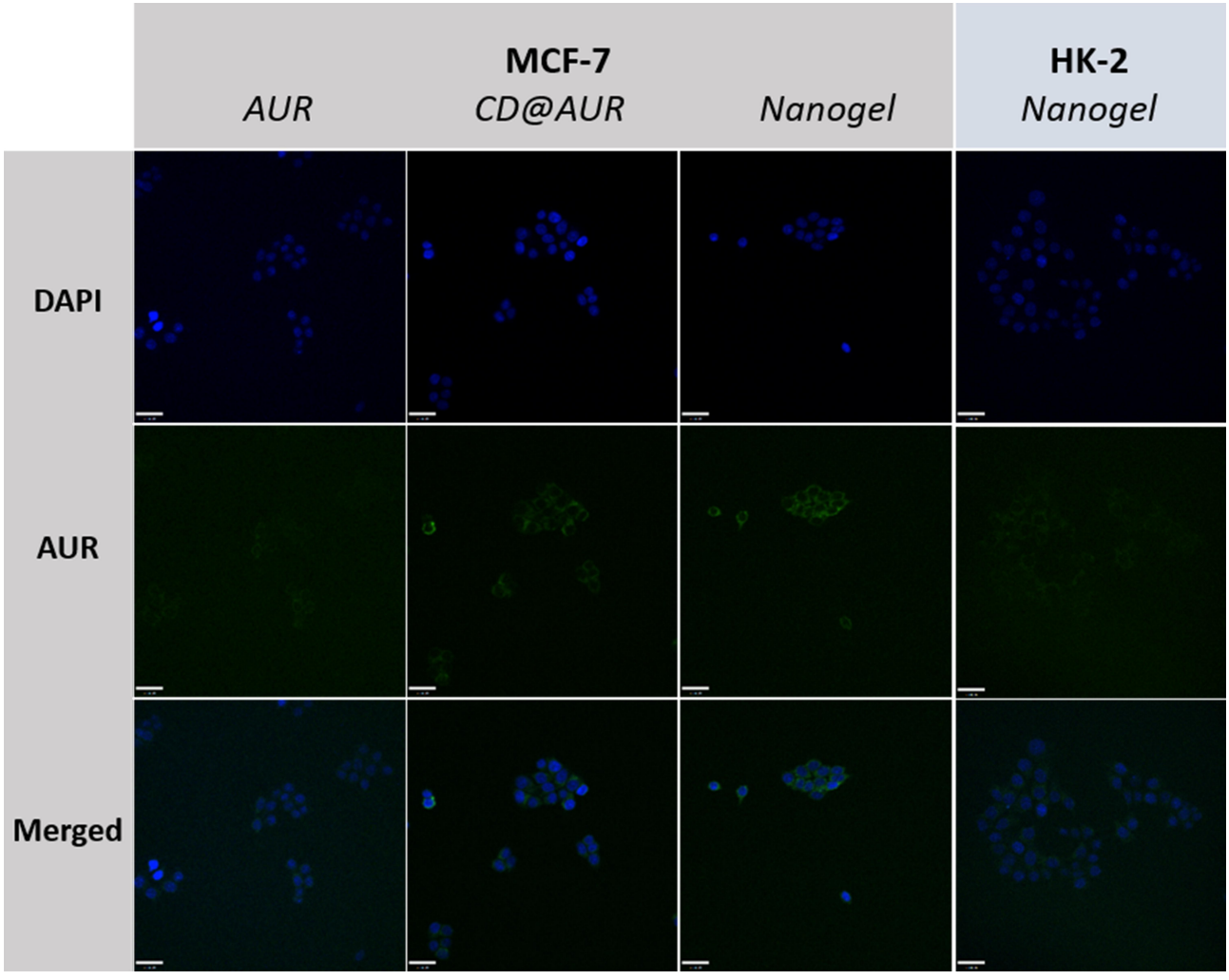

Figure 6 CLSM images of MCF-7 cells incubated with AUR, CD@AUR and the nanogel. To observe the selectivity, the nanogel was incubated with HK-2 cells under the same conditions.

@AUR, the cells treated with free AUR demonstrated very low fluorescence. The low fluorescence intensity of free AUR in cells may be due to its low bioavailability, solubility and selectivity affecting cell internalization.[20]

Selective Cytotoxicity of ^{CDDP}HA-CD@AUR

As mentioned above, ^{CDDP}HA-CD@AUR had a good optical effect, and the drug release was affected by the pH value. Therefore, it is necessary to evaluate whether the nanogel with HA as a carrier has selective cytotoxicity. The feasibility of ^{CDDP}HA-CD@AUR to selectively inhibit cell proliferation was verified by CCK-8 experiments. As shown in Figure 7, MCF-7 (tumor cells), MDA-MB -231 (tumor cells) and HK-2 cells (normal cells) were treated with different concentrations of ^{CDDP}HA-CD @AUR, free CDDP and the mixture of CDDP and AUR, respectively. It can be seen from the figure that free CDDP and the mixture have obvious cytotoxicity to normal cells and tumor cells. However, by comparing the graphs, it can be seen that, similar to 24 hours of culture with ^{CDDP}HA-CD@AUR, the cell viability of HK-2 cells was significantly higher than that of MCF-7 and MDA-MB-231 cells, and as the concentration of CDDP increased, the phenomenon became more obvious. When the CDDP concentration reached 10 μg/mL, the cell viability of HK-2 cells treated with the nanogel remained above 90%, while the corresponding tumor cells were below 70%. In Figure 7D, the cell viability of the nanogel treated HK-2 cells cells was higher than MCF-7 and MDA-MB-231 cells, and the trend becomes more obvious after 24 and 72 hours. These may be due to the lack of selectivity of free CDDP and

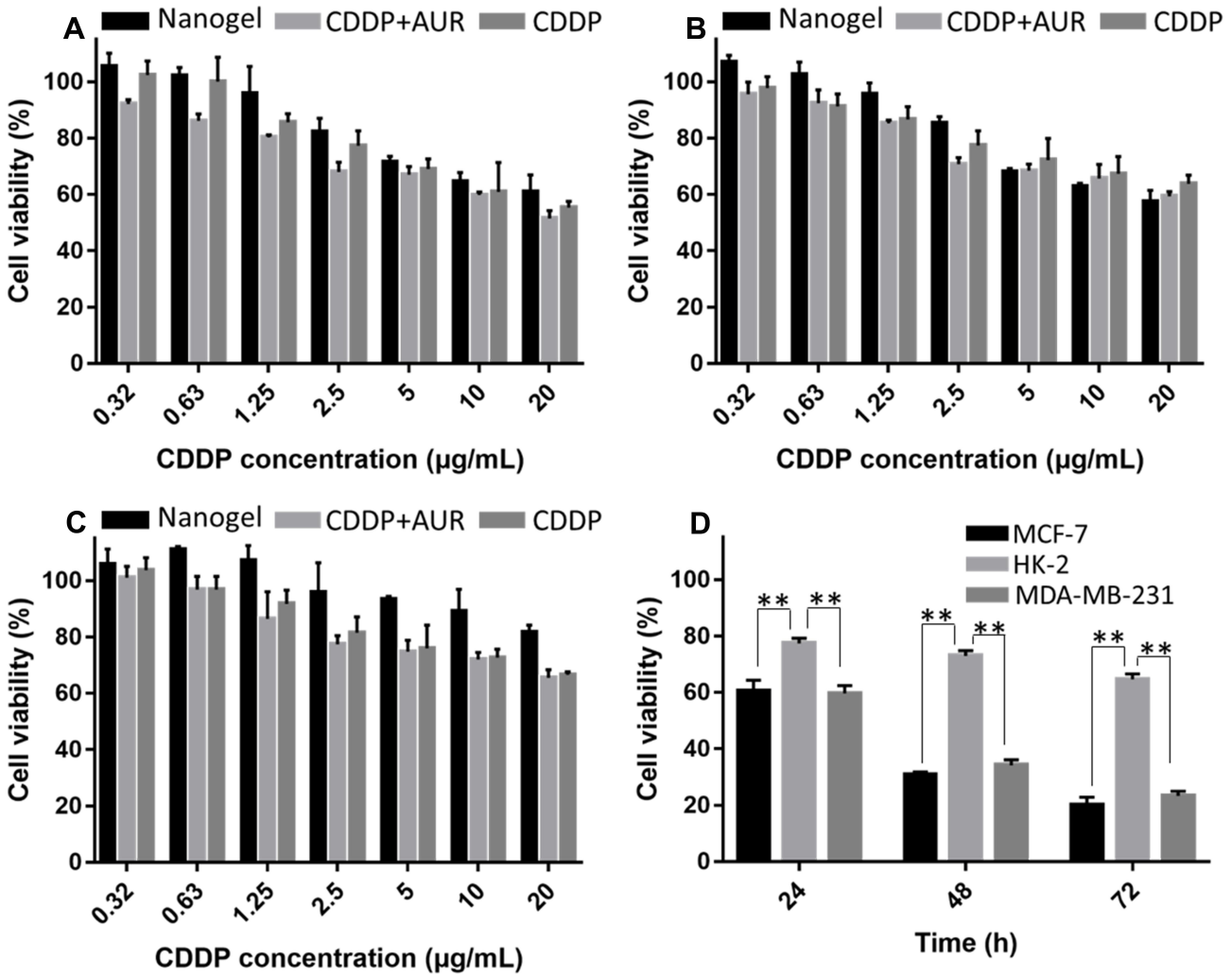

Figure 7 The cytotoxicity of CDDP, CDDP plus AUR and the nanogel against MCF-7 cells (**A**), MDA-MB-231 cells (**B**) and HK-2 cells (**C**). Cell viability of MCF-7, HK-2, and MDA-MB-231 cells incubated with the nanogel (**D**). *p < 0.05,**p < 0.01.

AUR, which can enter the cell membrane through rapid diffusion. After being loaded with HA to form a macromolecular compound, it can only enter cells by endocytosis, and it is necessary to promote drug release through the acidic environment inside the cell. Such results demonstrate the selectivity of HA-loaded CDDP and AUR in treating tumors.

To further verify the selectivity of the nanogel, the nanogel was cultured with MCF-7 cells and HK-2 cells, and the fluorescence was observed through CLSM. As shown in Figure 7, comparing the confocal images of MCF-7 cells and HK-2 cells, it can be seen that DAPI was evenly dispersed in the nucleus of the two cells, but the green light was significantly different. The fluorescence intensity in HK-2 cells was significantly lower than that in MCF-7 cells. Such results may be attributed to their different internalization mechanisms. CD44 receptors overexpressed on the surface of tumor cells can recognize HA, and the nanogel can enter cells in the form of endocytosis. The results were consistent with the CCK-8 experiment, indicating that the nanogel has selective cytotoxicity to tumor cells and has the potential to be used for tumor treatment in vivo.

In vivo Antitumor Efficiency

The BALB/C nude mice bearing MDA-MB-231 tumor xenografts were used as an animal model to study the antitumor effect of ^{CDDP}HA-CD@AUR in vivo. The tumor volume and body weight were recorded to evaluate the in vivo antitumor activity of the nanogel. As shown in Figure 8A, the control group was injected with 0.9% NaCl, and the tumor volume grew unlimitedly, while the tumor volumes of mice injected with free CDDP plus AUR and ^{CDDP}HA-CD@AUR were effectively controlled. The relative tumor volume growth of mice injected with free CDDP plus AUR and ^{CDDP}HA-CD @AUR became significantly slower, and both groups showed a tendency to become smaller during the administration process. Figure 8B shows that the trends of body weight change of the three groups were obviously different. The body weight of the mice injected with 0.9% NaCl slowly increased, and the nanogel injection decreased slightly, while the body weight of the mice injected with free CDDP plus AUR fell rapidly and one mouse died on the 10th day. These results indicate that the nanogel can effectively inhibit tumor growth and can also significantly reduce the systemic toxicity of drugs.

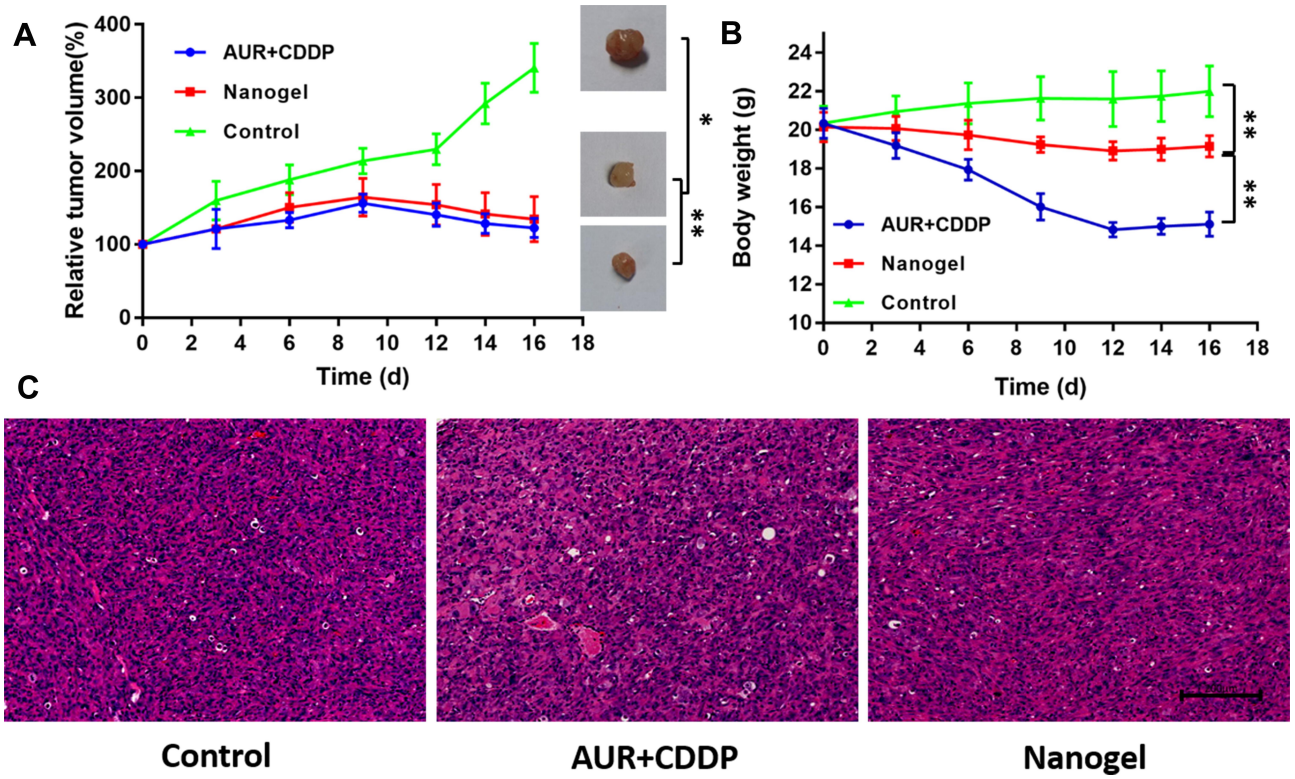

Figure 8 In vivo antitumor efficacy of MDA-MB-231 tumor-bearing mice treated with 0.9% NaCl, CDDP+AUR, and the nanogel. (**A**) The tumor volume evolution. (**B**) The body weight changes of mice. (**C**) H&E staining of the tumor sections. The data are shown as the mean±SD (n = 5), *p < 0.05,**p < 0.01. Scale bar: 200 μm.

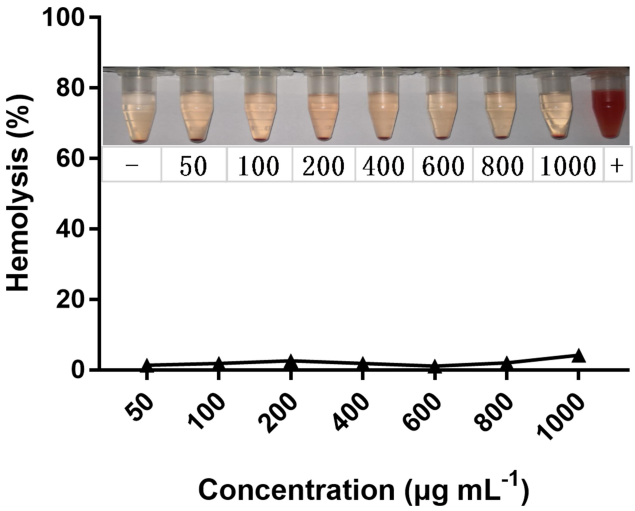

Figure 9 Percentage of hemolysis of RBCs incubated with ^{CDDP}HA-CD@AUR.

To further demonstrate the antitumor effect of the nanogel in vivo, the tumors of mice were isolated for histopathological analysis. As shown in Figure 8C, there was no obvious necrosis in the tumor slices of the control group, while the tumor slices of the mice treated with free CDDP plus AUR and the nanogel all showed damage. These results indicate that the nanogel can be selectively concentrated in tumor tissues and can be released in the acidic environment of tumors to exert antitumor effects.

In vivo Safety of ^{CDDP}HA-CD@AUR

^{CDDP}HA-CD@AUR has selective cytotoxicity to tumor cells and effectively inhibits the growth of tumors in vivo, therefore, it is essential to evaluate the safety of the nanogel. Poor blood compatibility may cause RBCs to rupture and lyse.[32] In this study, hemolysis experiment was used to estimate whether ^{CDDP}HA-CD@AUR is suitable for intravenous administration. As depicted in Figure 9, there was no obvious hemolysis in any concentration of ^{CDDP}HA-CD@AUR. When the concentration of ^{CDDP}HA-CD@AUR reached 1000 μg/mL, the hemolytic activity did exceed 5%. This result demonstrates that the nanogel exhibited excellent blood compatibility.

H&E staining of normal organs was performed to observe whether ^{CDDP}HA-CD@AUR caused systemic toxicity. As shown in Figure 10, normal organs in the control group showed no obvious morphological changes, and no obvious tissue necrosis, tissue damage or inflammatory infiltration was observed. However, varying degrees of tissue damage were observed in livers and kidneys treated with CDDP plus AUR. Compared with the ^{CDDP}HA-CD@AUR group, in liver tissue, the hepatic cords were arranged irregularly, and inflammation existed in the hepatic lobule. In the kidney tissue, the glomeruli were congested and inconsistent in size, while the tubular epithelial cells were disorderly arranged, and inflammatory

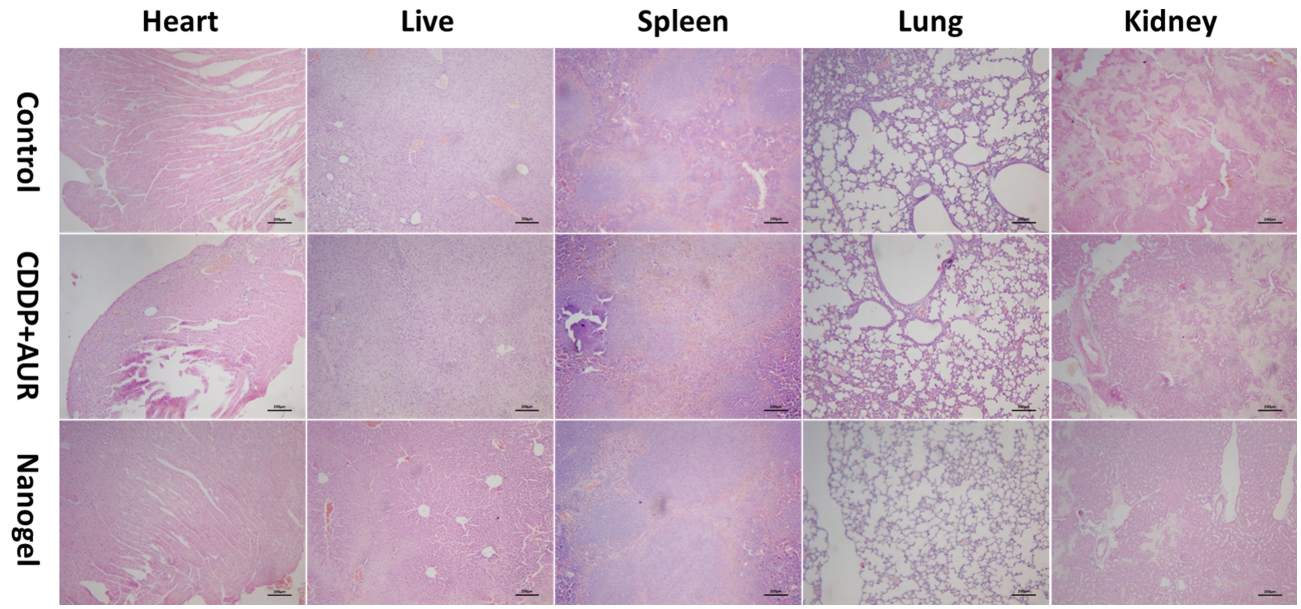

Figure 10 Histological analyses by H&E staining of heart, liver, spleen, lung, and kidney in BALB/C mice that were treated with 0.9% NaCl, CDDP+AUR, and the nanogel. Scale bar: 200 μm.

cell infiltration could be observed, indicating the occurrence of nephrotoxicity. In addition, the myocardial cell spaces of mice treated with free AUR plus CDDP were slightly filled with fibrous tissue. Interestingly, there was almost no obvious tissue damage in the tissues of mice treated with ^{CDDP}HA-CD@AUR. Such results indicate that the systemic toxicity of free AUR and CDDP was effectively reduced after being loaded into the nanogel.

Conclusions

A new nanogel, ^{CDDP}HA-CD@AUR, was prepared via chelate interactions for CDDP loading and host-guest interactions for AUR loading, respectively. The release of AUR and CDDP under tumor acidic microenvironment and intracellular lysosomal environment was significantly higher than that under normal physiological conditions, demonstrating that the release of drugs from the nanogel was pH-responsive. In addition, the nanogel can light up cells owing to its excellent optical properties after CD loading. Due to the overexpression of the HA receptor on the surface of tumor cells, the nanogel can be selectively internalized by MCF-7 cells in vitro, effectively inhibiting tumor growth and reducing system toxicity in vivo. Importantly, the nanogel exhibited excellent blood compatibility and physiological stability. Based on these, the nanogel with HA and CD as carriers has good potential for targeted delivery of AUR and CDDP against breast cancer.

Acknowledgment

This work was supported by Beijing Natural Science Foundation (7202111) and National Science and Technology Major Project (2018ZX10101001-005-003, 2018ZX10101001-005-004). All special thanks for the long-term subsidy mechanism from the Ministry of Finance and the Ministry of Education of PRC for BUCM.

Disclosure

The authors report no conflicts of interest for this work.

References

1. Lee JC, Shin EA, Kim B, et al. Auraptene induces apoptosis via myeloid cell Leukemia 1-mediated activation of caspases in PC3 and DU145 prostate cancer cells. *Phytother Res*. 2017;31:891–898. doi:10.1002/ptr.5810
2. Bibak B, Shakeri F, Barreto GE, Keshavarzi Z, Sathyapalan T, Sahebkar A. A review of the pharmacological and therapeutic effects of auraptene. *BioFactors*. 2019;45:867–879. doi:10.1002/biof.1550
3. Jalilzadeh N, Samadi N, Salehi R, et al. Novel nano-vehicle for delivery and efficiency of anticancer auraptene against colon cancer cells. *Sci Rep*. 2020;10:1606. doi:10.1038/s41598-020-58527-0
4. de Medina P, Genovese S, Paillasse MR, et al. Auraptene is an inhibitor of cholesterol esterification and a modulator of estrogen receptors. *Mol Pharmacol*. 2010;78:827–836. doi:10.1124/mol.110.065250
5. Krishnan P, Kleiner-Hancock H. Effects of auraptene on IGF-1 stimulated cell cycle progression in the human breast cancer cell line, MCF-7. *Int J Breast Cancer*. 2012;2012:502092. doi:10.1155/2012/502092
6. Hasan M, Genovese S, Fiorito S, Epifano F, Witt-Enderby PA. Oxyprenylated phenylpropanoids bind to MT1 melatonin receptors and inhibit breast cancer cell proliferation and migration. *J Nat Prod*. 2017;80:3324–3329. doi:10.1021/acs.jnatprod.7b00853
7. Jablonska K, Pula B, Zemla A, et al. Expression of melatonin receptor MT1 in cells of human invasive ductal breast carcinoma. *J Pineal Res*. 2013;54:334–345. doi:10.1111/jpi.12032
8. Lai L, Yuan L, Cheng Q, Dong C, Mao L, Hill SM. Alteration of the MT1 melatonin receptor gene and its expression in primary human breast tumors and breast cancer cell lines. *Breast Cancer Res Treat*. 2009;118:293–305. doi:10.1007/s10549-008-0220-1
9. Saboor-Maleki S, Rassouli FB, Matin MM, Iranshahi M. Auraptene attenuates malignant properties of esophageal stem-like cancer cells. *Technol Cancer Res Treat*. 2017;16:519–527. doi:10.1177/1533034616650119
10. Moussavi M, Haddad F, Rassouli FB, Iranshahi M, Soleymanifard S. Synergy between auraptene, ionizing radiation, and anticancer drugs in colon adenocarcinoma cells. *Phytother Res*. 2017;31:1369–1375. doi:10.1002/ptr.5863
11. Tanaka T, de Azevedo M, Durán N, et al. Colorectal cancer chemoprevention by 2 beta-cyclodextrin inclusion compounds of auraptene and 4′-geranyloxyferulic acid. *Int J Cancer*. 2010;126:830–840. doi:10.1002/ijc.24833
12. Chen Y, Chen Q, Zhu Q, et al. Small molecular theranostic assemblies functionalized by doxorubicin-hyaluronic acid-methotrexate prodrug for multiple tumor targeting and imaging-guided combined chemo-photothermal therapy. *Mol Pharm*. 2019;16:2470–2480. doi:10.1021/acs.molpharmaceut.9b00072
13. Zhang Y, Yang D, Chen H, et al. Reduction-sensitive fluorescence enhanced polymeric prodrug nanoparticles for combinational photothermal-chemotherapy. *Biomaterials*. 2018;163:14–24. doi:10.1016/j.biomaterials.2018.02.023
14. Chaurasia S, Patel R, Vure P, Mishra B. Oral naringenin nanocarriers: fabrication, optimization, pharmacokinetic and chemotherapeutic efficacy assessments. *Nanomedicine (London, England)*. 2017;12:1243–1260. doi:10.2217/nnm-2016-0436
15. El-Shishtawy RM, Oliveira AS, Almeida P, Ferreira DP, Conceicao DS, Ferreira LF. Photophysical studies of a new water soluble indocarbocyanine dye adsorbed onto microcrystalline cellulose and beta-cyclodextrin. *Molecules*. 2013;18:5648–5668. doi:10.3390/molecules18055648
16. Bai L, Yan H, Bai T, et al. High Fluorescent Hyperbranched Polysiloxane Containing β-Cyclodextrin for Cell Imaging and Drug Delivery. *Biomacromolecules*. 2019;20:4230–4240. doi:10.1021/acs.biomac.9b01217
17. McFadden P, Frederick K, Argüello L, et al. UV fluorescent epoxy adhesives from noncovalent and covalent incorporation of coumarin dyes. *ACS Appl Mater Interfaces*. 2017;9:10061–10068. doi:10.1021/acsami.6b13218
18. Xie X, Tang F, Shangguan X, et al. Two-photon imaging of formaldehyde in live cells and animals utilizing a lysosome-targetable and acidic pH-activatable fluorescent probe. *Chem Commun*. 2017;53:6520–6523.
19. Iliopoulos K, Krupka O, Gindre D, Sallé M. Reversible two-photon optical data storage in coumarin-based copolymers. *J Am Chem Soc*. 2010;132:14343–14345. doi:10.1021/ja1047285
20. Roozbehi S, Dadashzadeh S, Mirshahi M, Sadeghizadeh M, Sajedi RH. Targeted anticancer prodrug therapy using dextran mediated enzyme-antibody conjugate and beta-cyclodextrin-curcumin inclusion complex. *Int J Biol Macromol*. 2020;160:1029–1041. doi:10.1016/j.ijbiomac.2020.05.225

21. DeDora DJ, Suhrland C, Goenka S, et al. Sulfobutyl ether beta-cyclodextrin (Captisol((R))) and methyl beta-cyclodextrin enhance and stabilize fluorescence of aqueous indocyanine green. *J Biomed Mater Res B Appl Biomater*. 2016;104:1457–1464. doi:10.1002/jbm.b.33496
22. Alam MM, Han HS, Sung S, et al. Endogenous inspired biomineral-installed hyaluronan nanoparticles as pH-responsive carrier of methotrexate for rheumatoid arthritis. *J Control Release*. 2017;252:62–72. doi:10.1016/j.jconrel.2017.03.012
23. Lee J, Chung S, Cho H, Kim D. Iodinated hyaluronic acid oligomer-based nanoassemblies for tumor-targeted drug delivery and cancer imaging. *Biomaterials*. 2016;85:218–231. doi:10.1016/j.biomaterials.2016.01.060
24. Li Q, Chen Y, Zhou X, et al. Hyaluronic acid-methotrexate conjugates coated magnetic polydopamine nanoparticles for multimodal imaging-guided multistage targeted chemo-photothermal therapy. *Mol Pharm*. 2018;15:4049–4062. doi:10.1021/acs.molpharmaceut.8b00473
25. Sargazi A, Kamali N, Shiri F, Heidari Majd M. Hyaluronic acid/polyethylene glycol nanoparticles for controlled delivery of mitoxantrone. *Artif Cells Nanomed Biotechnol*. 2018;46:500–509. doi:10.1080/21691401.2017.1324462
26. Zhang Y, Wang F, Li M, et al. Self-stabilized hyaluronate nanogel for intracellular codelivery of doxorubicin and cisplatin to osteosarcoma. *Advan Sci*. 2018;5:1700821. doi:10.1002/advs.201700821
27. Shirbin S, Ladewig K, Fu Q, et al. Cisplatin-induced formation of biocompatible and biodegradable polypeptide-based vesicles for targeted anticancer drug delivery. *Biomacromolecules*. 2015;16:2463–2474. doi:10.1021/acs.biomac.5b00692
28. Huynh V, Chen G, de Souza P, Stenzel M. Thiol-yne and thiol-ene "click" chemistry as a tool for a variety of platinum drug delivery carriers, from statistical copolymers to crosslinked micelles. *Biomacromolecules*. 2011;12:1738–1751. doi:10.1021/bm200135e
29. Xu C, Wang Y, Guo Z, et al. Pulmonary delivery by exploiting doxorubicin and cisplatin co-loaded nanoparticles for metastatic lung cancer therapy. *J Control Release*. 2019;295:153–163. doi:10.1016/j.jconrel.2018.12.013
30. Wang Z, Yu Y, Dai W, et al. The use of a tumor metastasis targeting peptide to deliver doxorubicin-containing liposomes to highly metastatic cancer. *Biomaterials*. 2012;33:8451–8460. doi:10.1016/j.biomaterials.2012.08.031
31. Xiao K, Li Y, Luo J, et al. The effect of surface charge on in vivo biodistribution of PEG-oligocholic acid based micellar nanoparticles. *Biomaterials*. 2011;32:3435–3446. doi:10.1016/j.biomaterials.2011.01.021
32. Sun D, Ding J, Xiao C, Chen J, Zhuang X, Chen X. Preclinical evaluation of antitumor activity of acid-sensitive PEGylated doxorubicin. *ACS Appl Mater Interfaces*. 2014;6:21202–21214. doi:10.1021/am506178c
33. Lou C, Tian X, Deng H, Wang Y, Jiang X. Dialdehyde-beta-cyclodextrin-crosslinked carboxymethyl chitosan hydrogel for drug release. *Carbohydr Polym*. 2020;231:115678. doi:10.1016/j.carbpol.2019.115678
34. Xiong S, Wang Z, Liu J, et al. A pH-sensitive prodrug strategy to co-deliver DOX and TOS in TPGS nanomicelles for tumor therapy. *Colloids Surf B Biointerfaces*. 2019;173:346–355. doi:10.1016/j.colsurfb.2018.10.012
35. Du J-Z, Du X-J, Mao C-Q, Wang J. Tailor-made dual pH-sensitive polymer–doxorubicin nanoparticles for efficient anticancer drug delivery. *J Am Chem Soc*. 2011;133:17560–17563. doi:10.1021/ja207150n
36. Pei M, Pai JY, Du P, Liu P. Facile synthesis of fluorescent hyper-cross-linked beta-cyclodextrin-carbon quantum dot hybrid nanosponges for tumor theranostic application with enhanced antitumor efficacy. *Mol Pharm*. 2018;15:4084–4091. doi:10.1021/acs.molpharmaceut.8b00508
37. Liu W, Liu H, Peng X, et al. Hypoxia-activated anticancer prodrug for bioimaging, tracking drug release, and anticancer application. *Bioconjug Chem*. 2018;29:3332–3343. doi:10.1021/acs.bioconjchem.8b00511-#